

**SINGLE-CELL RNA-SEQ ANALYSIS OF AN LGR6+ EPIDERMAL STEM CELL
LINEAGE-TRACED TISSUE EXPANSION MODEL**

by
Chenyi Lyu

A thesis submitted to Johns Hopkins University in conformity with the requirements for the
degree of Master of Science in Engineering

Baltimore, Maryland

April 2021

© 2021 Chenyi Lyu

All rights reserved

Abstract

Mechanical input is a key element for guiding cell behavior in mammalian skin and regulating dermal development (Romani et al., 2020). The molecular mechanism underlying this instructive role has been investigated extensively. However, most studies that have examined the association between mechanical forces and tissue development have been restricted to in vitro systems. Some experiments have probed in vivo models, but our understanding of the driving mechanism and cellular heterogeneity remains limited. To obtain a comprehensive cellular survey of how mechanical forces drive skin growth, here, we designed an in vivo lineage-traced system with a single-cell RNA-seq approach that allows us to dissect the process at single-cell resolution. With the reconstructed gene expression programs, we identified the common transcriptional pattern and the physiologic process implicated in the expansion state of the epidermis. We show that the epidermal compartment responds quite heterogeneously to stretch and that Lgr6 cells compose the lineage that commits to new skin generation. Further exploration of gene expression level and trajectory inference confirm that the key regulator YAP1 suppresses the Hippo pathway, which normally constrains tissue growth, and activates downstream cell proliferation and differentiation pathways. Our study provides a systematic overview of epidermal cellular change on the single-cell level, potentially revealing rich information for therapeutic manipulation.

Primary Reader and Advisor: Luis A. Garza

Secondary Reader: Sashank Reddy; Yingchao Xue

Acknowledgement

I am very grateful to my advisor Luis Garza, Sashank Reddy, and my lab leader Yingchao Xue for the guidance alongside the path of my Master study. Huge thank you from me to each one in my family, of my friends and Ran's cat River who has supported me during this unusual year and will always be on my side down the road. Thank you all.

Wish everyone have a big bright future.

Contents

Abstract	ii
Acknowledgement	iii
List of figures	v
Introduction	1
Methods	3
scRNA-seq data preprocessing and quality control	3
Gene set enrichment analysis and gene ontology analysis.....	3
Gene scoring analysis	4
Pseudotime and trajectory inference	4
Results and Discussion.....	5
scRNA-seq identifies different skin cell types and the changes they undergo during skin...	5
Deconstructing the expansion state of epithelial cell clusters	9
Expansion leads to heterogeneity in the skin stem cell niche	12
Replenishment and regeneration of the skin epidermis is driven by different stem cell.....	13
Pseudotemporal trajectory analysis reveals Lgr6 stem cell plasticity during skin	15
Conclusion	18
References.....	19

List of figures

Figure 1 Single-cell RNA-seq reveals different skin cell types and how they change during expansion	7
Figure 2 Deconstructing the expansion state of epithelial cell clusters	11
Figure 3 Heterogeneity in the skin stem cell niche in response to expansion	14
Figure 4 Pseudo-temporal trajectory analysis reveals Lgr6+ stem cell plasticity during skin expansion	17

Introduction

The epithelial tissue experiences frequent mechanical forces during development and homeostasis. Mechanical forces are considered to be one of the major instructive signals in shaping the tissue environment and directing cell fate. Generally, these cues can directly or indirectly change the physical property of the extracellular matrix, neighboring cells, and cell conformation (Romani et al., 2020), 2020). Mechanical stimuli are received by the cells and transmitted into biochemical signals via multiple mechanosensors (e.g., focal adhesion and cell-cell junctions) on the cell surface. The signals subsequently alter physiologic processes, including cell proliferation, apoptosis, and differentiation (Iskratsch et al., 2014) ratsch et al., 2014). However, it is not yet understood how the complex orchestration is coordinated among and within cells.

Skin is the largest yet most accessible organ in mammals. Therefore, it serves as an elegant model system to study. The maintenance of skin epithelium through cellular turnover relies largely on the plasticity of stem cells resident in distinct niches (Fuchs, 2008; Ito et al., 2005). For skin regeneration, mechanical force-mediated expansion serves as a key regulator in a variety of contexts. For example, in a physiologic scenario, mechanical forces are instrumental in the transformation of abdominal shape during pregnancy, and in practical applications, expanders are used in reconstructive surgery to generate new skin (Neumann, 1957). Although this phenomenon has been applied for over 70 years, many fundamental questions remain: How is the mechanical signal transmitted to cells? How do cells convert the physical force into biological signals? How do the cells adapt to mechanical cues? What is the cell of origin for the new skin? How does each skin compartment coordinate spatially at a molecular level in response to the stimuli?

Studies of cellular behavior in mechanical biology have been based primarily on in vitro experiments, which have yielded important discoveries, such as the regulation networks involved and how nuclei adapt to stretch. Although the mechanical parameters are relatively easy to control and modulate in vitro, these systems are not easy to fully recapitulate in an in vivo microenvironment (Nava et al., 2020; Tang et al., 2013). The advances of single-cell RNA sequencing make it possible to probe transcriptomic changes and infer physiologic changes at the single-cell resolution. One recent study used this technology to investigate stretch-mediated skin expansion in mouse. The authors found distinct states of basal cells during the tissue expansion (Aragona et al., 2020). This finding raises interesting subsequent questions: do the distinct compartments within the epidermis respond and adapt to expansion in a common transcriptome?

Recently, advances in machine learning algorithms have enabled us to mine the single-cell transcriptome more thoroughly and examine cellular behaviors in a detailed manner (Butler et al., 2018; Macosko et al., 2015; Street et al., 2018; Van den Berge et al., 2020). Importantly, we have developed a tailored stem cell lineage-traced mouse system that allows us to finely stimulate mechanical conditions in vivo and study the process for up to 2 months. In this study, we combined a genetic approach with single-cell sequencing to identify the heterogeneity among epidermal cells during the response to expansion. We confirmed that Lgr6+ cells commit to the lineage of newly generated skin under modulation of the pivotal regulator YAP1. Furthermore, we show that Lgr6+ progeny take on an enhanced stem cell state and adapt interfollicular epidermis (IFE)-like characteristics on the pseudotemporal axis. Overall, our study provides a single-cell perspective of epidermal cellular dynamics and biological function during mechanically induced skin regeneration.

Methods

scRNA-seq data preprocessing and quality control

We have two batches of data for a total of 4 samples, with each sample consisting of 3 biological replicates. After the initial cell ranger metric assessment, data were preprocessed with the Seurat package (Macosko et al., 2015). We kept cells with more than 500 unique molecular identifiers (UMI), 200 genes, 0.7 cell complexity ($\log_{10}\text{GenePerUMI}$), and less than 0.1 mitochondria gene ratio and filtered out genes that were expressed in fewer than 10 cells.

After quality control, 15,802 cells with 17,022 genes remained and were used for clustering. Briefly, single-cell data matrices were first normalized and log transformed. For each sample, cell cycle phases were calculated and assigned by using the CellCycleScoring function of the software. To remove unwanted sources of variability caused by differences in cycling stages and mitochondrial ratio, we set the variable.features.n to be 3000, and included mitoRatio, S.scores and G2/M.score in vars.to.regress. Next, to ensure that similar cells across the conditions were clustered, we used the top 3,000 highly variable genes for canonical correlation analysis implemented in Seurat to align and integrate the full dataset. Principal component analysis was performed first, and the top 20 PCs (principal components) out of 40 pcs with resolution 0.45 were selected to obtain 16 clusters. By visualizing the established epithelial cell markers from literature on the feature plot, we identified 13 clusters for downstream analysis.

Gene set enrichment analysis and gene ontology analysis

Gene ontology analysis of differentially expressed genes for pseudobulk data was performed by gprofiler2 (<https://biit.cs.ut.ee/gprofiler/page/r>). Representative terms were selected from top-ranked gene sets/pathways. For gene set enrichment analysis, all differentially expressed genes

were first evaluated by Wilcoxon rank sum test (function `wilcoxauc` in `presto`). The queried database included MSigDB: CP: KEGG, CP: REACTOME, and Hallmark.

Gene scoring analysis

To calculate gene scores for selected molecular signatures, we acquired gene sets from the MSigDB database and published literature. The `AddModuleScore` function in the `Seurat` R package was then used to calculate the average expression level of each gene set for each cluster on a single-cell level. The two-sided Wilcoxon rank sum test was adapted to determine whether there was a significant difference between the evaluated signature scores of two groups.

Pseudotime and trajectory inference

We adopted the analysis procedure from an online resource (<https://kstreet13.github.io/bioc2020trajectories/articles/workshopTrajectories.html>). We performed pseudotemporal ordering of Lgr6+ (progenitor) and tdTomato+ (Lgr6 progeny) cells, including spinous cells, non-proliferating basal cells, infundibulum, HF III, and HF IV cells. Briefly, we assessed imbalanced score, which helps to determine if local cell distribution is balanced as compared to global cell distribution. Next, we performed trajectory inference using cells from both conditions in Slingshot. The `fitGAM` function in `tradeSeq` was applied (`nKnot = 5`) to estimate a smooth expression profile for the top 2,000 variable genes derived from `Seurat` `FindVariableFeature`. The null hypothesis was used to test whether the association of gene expression change with the pseudotime was significant..

Results and Discussion

scRNA-seq identifies different skin cell types and the changes they undergo during skin expansion

To systematically investigate the cell-type-specific changes that occur during mechanically induced skin expansion at a single-cell level, we performed scRNA-seq on samples isolated from nonexpanded (NE) and expanded (E) lineage-traced mice (Lgr6-EGFP-Ires-CreERT2 crossed with R26-tdTomato reporter mice) (Barker et al., 2007; Madisen et al., 2010; Snippert et al., 2010). We induced Tomato lineage tracing of Lgr6+ cells by administering tamoxifen to 8-week-old expander-implanted male mice 1 week before the expansion was completed. We isolated keratinocytes from the skin over the expander at the PD0 (post-expansion day 0) time point. We sorted the live cells by flow cytometry and submitted them for scRNA-seq. After filtering out low-quality cells, we obtained 8,479 epithelial cells from NE samples and 6,570 epithelial cells from E samples for downstream analysis. We integrated and clustered all cell samples using Seurat. By visualizing known cell-type-specific marker expression on feature plots, we identified seven major cell types, including spinous cell (Krt1+, Krt10+), basal cell (Krt14+, Krt5+), proliferating basal cell (Mki67+, Krt14+, Krt5+), hair-follicle-associated cell (HF, Krt15+, Krt17+, Krt79+), hair follicle stem cell (HFSC, Lgr5+, Cd34+), sebaceous gland (Mgst1+, Scd1+), and immune cell (Cd3d+, Cd207+) (Figure 1A, C, G) (Haensel et al., 2020; Joost et al., 2020; Joost et al., 2016). Cell type distribution statistics show that spinous cells were more numerous than basal cells in the E sample (Figure 1B), consistent with our findings from hematoxylin & eosin staining. Moreover, cell population percentages entering into the G2M phase were increased in the E sample (Figure 1D). These results are consistent with morphologic analysis and immunofluorescence staining (Mki67, Krt17), suggesting that the epidermis of expanded skin is undergoing hyper-proliferation and thus thickening.

We then examined NE and E samples separately and contrasted their transcriptome program. Cell type and feature gene expression in each subcluster of the two conditions showed general consistency with those of previous studies (Haensel et al., 2020; Joost et al., 2020). Although the NE and E samples had common molecular features, some genes were distinctly enriched in the E sample. Differential gene expression analysis revealed unique transcriptional features in the expansion state (Figure 1E). Some genes were much more highly expressed in the E sample, including inflammation-related genes (S100a8, S100a9) (Cheng et al., 2018); the pro-inflammatory transcript Stfa3 (Gao et al., 2012); the keratinocyte differentiation-associated gene Sprr2a3 (Tong et al., 2006); and a subunit of the metabolic enzyme Ndufa4l2 (Tello et al., 2011). Additionally, the E sample was characterized by downregulation of hair follicle cell marker Krt15; Mt4; cell motility mediator Malat1 (Gutschner, 2013); hemostasis regulator Hopx; keratin-encoding gene Krt77; and chemokine ligand Ccl27a. The alterations in gene expression suggest an underlying change in cell cluster distribution and biological processes (Toruner et al., 2004). Gene ontology analysis of the upregulated genes ($n = 121$, $|avg_logFC| > 0.25$ and $p_val_adj < 0.05$) showed that the E sample was undergoing an intense metabolic process and hypoxia response. The downregulated genes that we identified ($n = 77$) were associated with cell junction, focal adhesion, and negative regulation of cell proliferation, as supported by our microarray data (Figure 1F). Taken together, these results indicate that the gene programs captured are robust to study and that expansion induces global changes in the epidermis.

Figure 1 scRNA-seq reveals different skin cell types and how they change during skin expansion

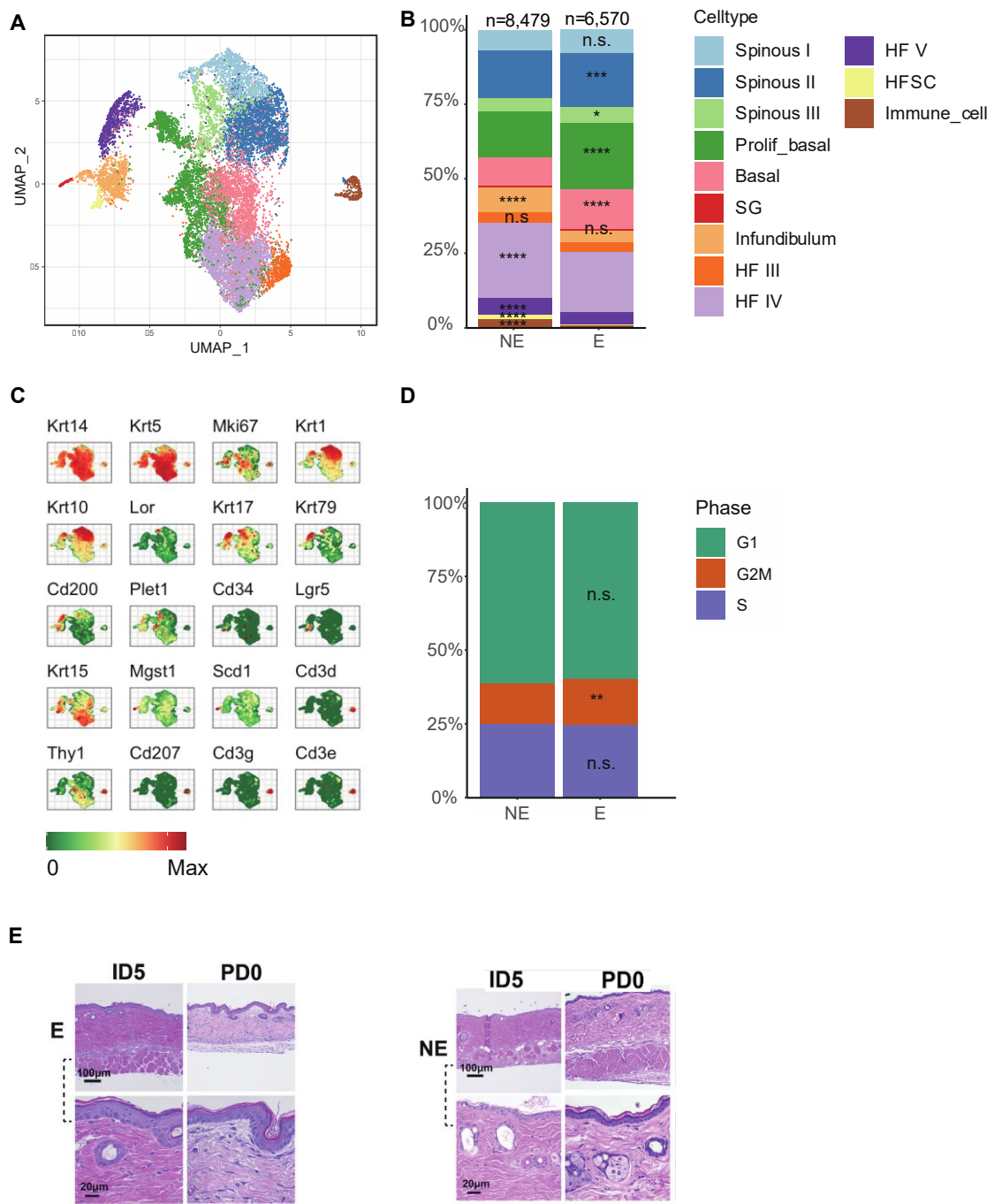


Figure 1. scRNA-seq reveals different skin cell types and how they change during skin expansion.

(A) Uniform manifold approximation and projection plot for full epidermal cells from samples isolated from nonexpanded (NE) and expanded (E) lineage-traced mice show 12 cell clusters ($n = 8,479$ for NE and $6,570$ for E). Colors corresponding to each cell type are shown in panel B.

(B) Bar plot illustrating cell components in each sample. A chi-square test was performed (* $p < 0.05$; ** $p < 0.01$; *** $p < 0.001$; **** $p < 0.0001$; n.s. > 0.05).

(C) Feature plot showing the expression level of established cell type markers used to identify cell clusters.

(D) Bar plot illustrating cell phase constitution in each sample. A chi-square test was performed (** $p < 0.01$).

(E) Histology change showing skin layers.

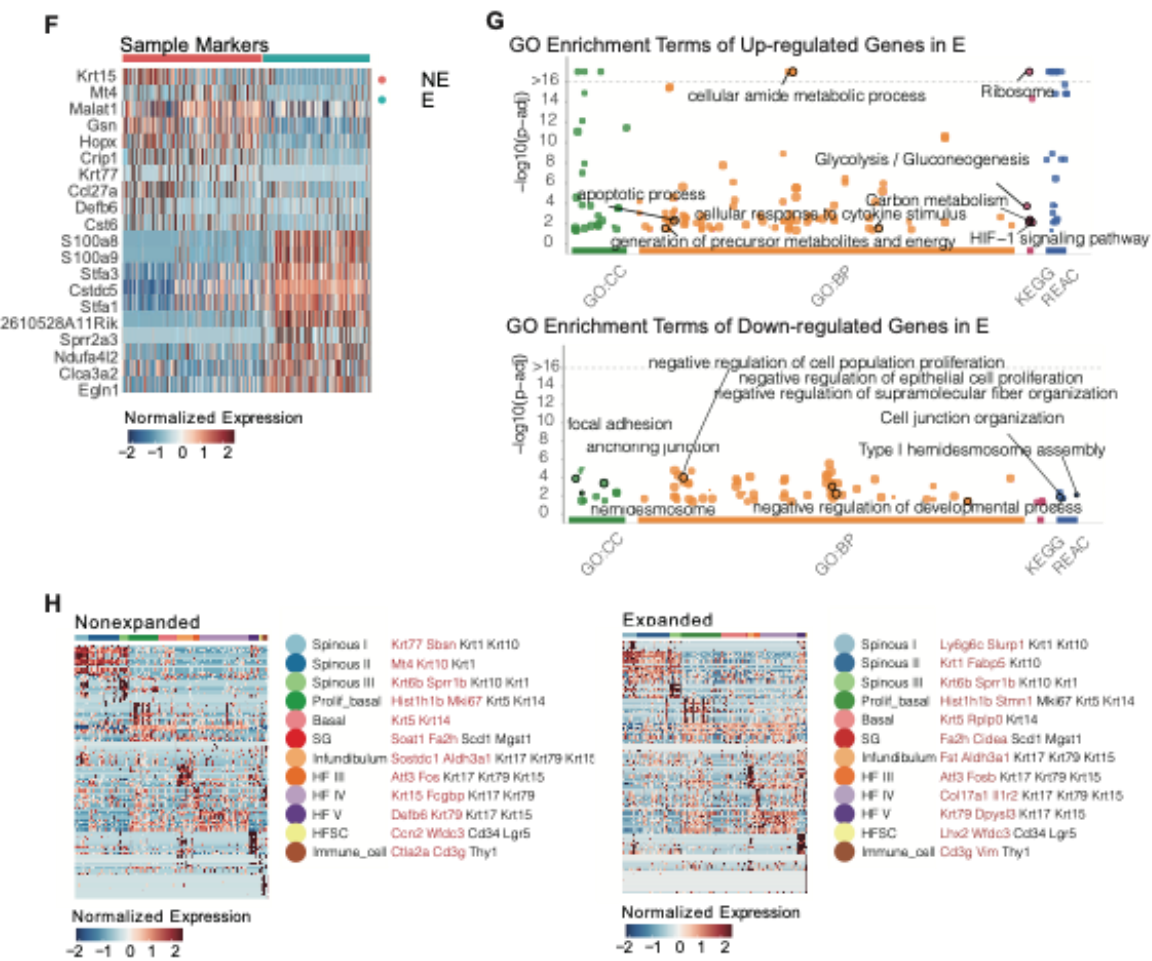


Figure 1. (con'd) scRNA-seq reveals different skin cell types and how they change during skin expansion.
(F) Heatmap for the top 10 condition feature genes in the NE and E samples.

(G) Manhattan plot highlights the selected gene ontology (GO) terms using the top E upregulated genes (171 differentially expressed genes) and downregulated genes (77 differentially expressed genes) (BP: biological process, CC: cellular components, REAC: Reactome).

(H) Heatmaps for the top 10 cluster feature genes in NE and E samples. Genes listed in black represent the top two marker genes for each cluster, whereas those in red represent the additional genes used in the final identification of the cluster cell type.

Deconstructing the expansion state of epithelial cell clusters

Next, we sought to define the common gene expression patterns activated in major epidermal cell clusters by mechanically induced expansion. We excluded minor cell clusters (sebaceous gland and immune cells) and divided the major cell clusters into three groups: basal group, spinous group, and hair follicle (HF) group. We found hundreds of genes that were differentially expressed between cells in the E and NE states. We identified 142 differentially expressed genes that were upregulated in the basal group, 104 in the spinous group, and 194 in the HF group. By comparison, 230, 227, and 161 differentially expressed genes were downregulated in those three groups, respectively (Figure 2A, B). Notably, gene ontology analysis of the shared enriched genes ($n = 64$) revealed that the expansion state is associated with enhanced metabolism and catabolism (Figure 2C). In the basal and HF groups, the physiologic processes identified were related to inflammatory responses and cellular responses to stimuli. The underlying molecular signature involved upregulation of fatty acid binding, amino acid metabolism, and gluconeogenesis. GTPases, which activate NADPH oxidases and are part of a key pathway in signal transduction, were uniformly upregulated in the basal and spinous groups. Previous studies have indicated that mechanical cues regulate cell metabolism via extracellular matrix–cell and cell–cell crosstalk (Green, 1977; Gurkar et al., 2013; Pedersen et al., 2012). Our findings support current knowledge and reveal the heterogeneity of induced biological processes in the skin epidermis at the cellular level.

Because mechanically induced skin expansion is generally observed in organ development, we then examined expression of components of the Hippo pathway, a pivotal intracellular signaling pathway that restricts organ size and tissue growth, in the major epidermal cell groups (Figure 2D; (Dobrokhotov et al., 2018)). Pathway score analysis showed consistent repression of the Hippo pathway in E epidermal cell groups, indicating that the limitation on tissue growth had

been blocked. Activation of the Hippo signaling pathway depends strongly on cell junctions and the phosphatidyl inositol-3-kinase (PI3K) signaling pathway, which cooperates with the Hippo pathway to mediate cell proliferation, cell growth, and cell apoptosis (Borreguero-Muñoz et al., 2019; Karaman and Halder, 2018). These two Hippo-related pathways were also downregulated in the expansion state. Collectively, these data highlight distinct transcriptome programs and functional signatures associated with activation and induction of metabolic priming and cell proliferation among epidermal cells during tissue expansion.

Notably, genes related to glycolysis and the response to hypoxia were strikingly upregulated in the HF group after expansion. Interestingly, we found that the gene for the key regulator of the Hippo pathway, YAP1, rather than the co-activator Wwtr1, was solely and highly induced by expansion in the HF group (Figure 3C). Usually, when Hippo pathway-related tissue overgrowth occurs, YAP and TAZ proteins cooperate and activate the downstream cell progression-related cascade (Dobrokhotov et al., 2018). The downstream growth-promoting gene Myc and cell migration-related gene Amotl1 were also elevated. As expected, representative genes involved in Hippo-related pathways, such as Itgb1, Vcl, and Hif1a, were upregulated significantly. Moreover, gene scoring captures cells included in HF group behaves differently for PI3K signaling and adherens junction. After expansion, the expression score across cell population tends to be converged and repressed to a uniform level. This finding suggests that the YAP-Hippo pathway is disturbed in the HF group. Importantly, different states and responses may exist in HF cell subsets during homeostasis and expansion states.

Figure 2 Deconstructing the expansion state of epithelial cell clusters

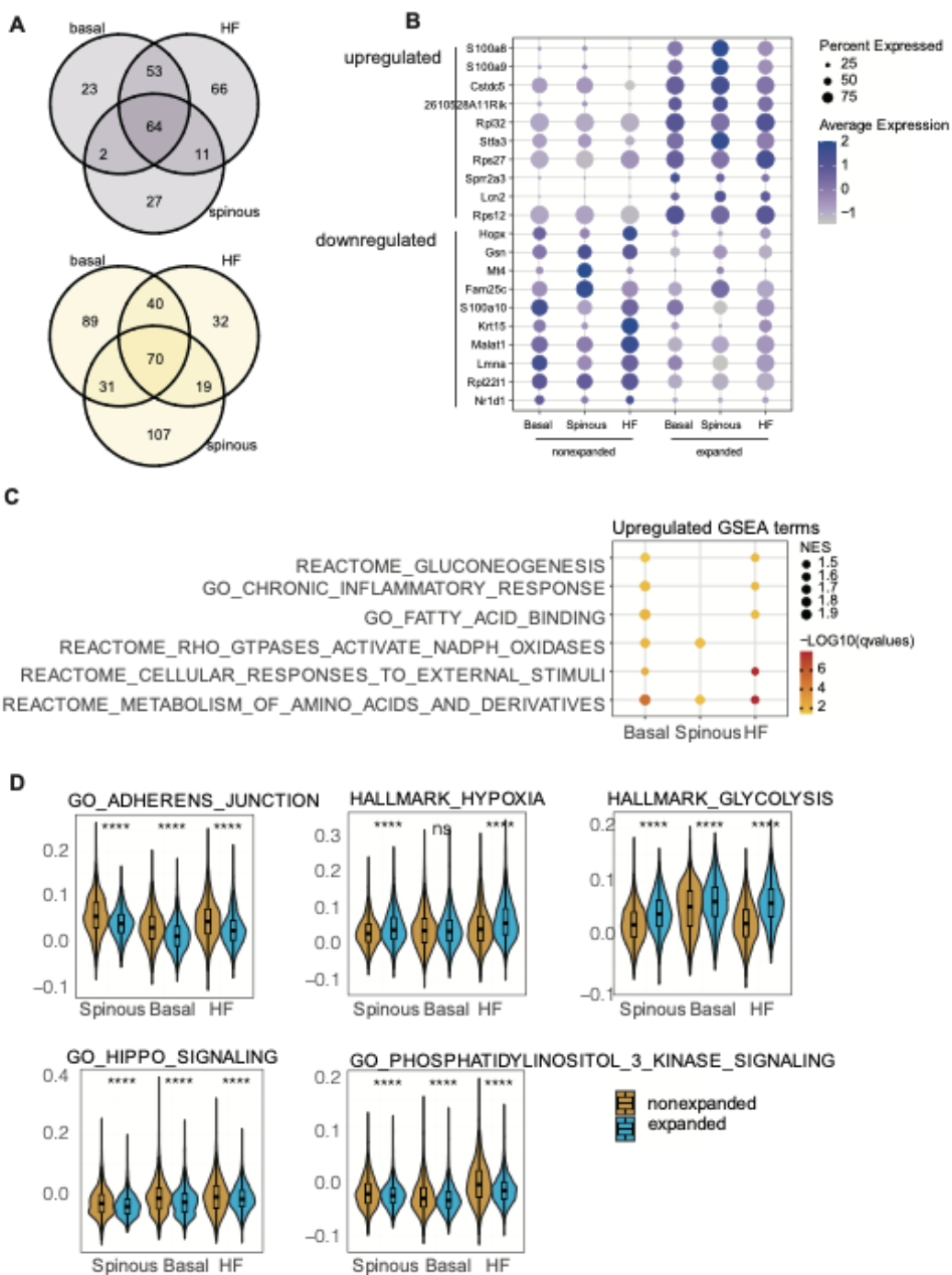


Figure 2. Deconstructing the expansion state of epithelial cell clusters.

(A) Venn diagram displaying the number of shared upregulated (top) and downregulated (bottom) differentially expressed genes (DEGs, $|avg_logFC| > 0.25$ and $p_val_adj < 0.05$) for the main epithelial cell types. HF, hair follicle cells.

(B) Dot plot highlights the top 10 shared feature DEGs (DEGs, $|avg_logFC| > 0.25$ and $p_val_adj < 0.05$) in the main epithelial cell types.

(C) Representative shared gene ontology (GO) terms of expansion-associated DEGs in the main epithelial cell types. NES indicates the normalized enrichment score. The color bar that ranges from yellow to red indicates the range of $-log\ q$ values.

(D) Gene set scoring analysis using the selected molecular signatures in the main epithelial cell types. p values are from two-sided Wilcoxon rank-sum tests. *** $p < 0.0001$; n.s. > 0.05 .

Expansion leads to heterogeneity in the skin stem cell niche

The HF compartment accommodates distinct types of stem cell populations and is one source for skin regeneration. Having observed signs of different responses to expansion among HF subpopulations, we next explored the heterogeneity in HF cells. From the previous classification, we observed five subpopulations in the NE sample (Figure 3A): (1) an infundibulum subpopulation enriched for a set of infundibulum markers (*Fst*, *Sostdc1*, *Krt79*, *Krt17*), as defined in prior literature (Haensel et al., 2020; Joost et al., 2016).; (2) an HFIII subpopulation enriched for transcription activation and early response genes such as *Fos*, *Jun*, and *Atf3*, which are associated with promoting neuron regeneration and cell proliferation; (3) an HF subpopulation that exhibited a stepwise increase in expression of collagen *Col17a1*, IFE signature *Krt5*, and *Krt14* in which HFIV was the most outstanding subcluster; (4) an HFV subpopulation that highly expressed a set of upper HF markers, such as *Cst6*, *Krt79*, and *Defb6*; and (5) an HF stem cell population characterized by Bu-HFSC signature *Wfdc3* and *Cxcl14*. These subpopulations had feature genes that overlapped with those that have been previously reported (Haensel et al., 2020; Joost et al., 2016). Taking advantage of our labeling model, we found that the expression of *Lgr5*, *Lgr6*, and *TdTomato* corresponded to the staining. Our samples showed a large percentage of *tdT+* cells in the infundibulum after expansion. Moreover, by examining the feature expression in the E sample, we found a high level of similarity in the shared gene expression pattern for the corresponding subpopulation between the two conditions (Figure 3B). Therefore, the defined subpopulations were robust in our sample data.

The defined subclusters had distinct molecular signatures (Figure 3D). During homeostasis, HFSC and HFIII scored higher in Hippo signaling and hypoxia; by contrast, the other three subpopulations scored lower, and HFV was the lowest. HFSC is the population that has the highest stemness and quiescence, whereas quiescence score exhibits a stepwise decrease

from infundibulum to HFIV (Cheung and Rando, 2013). The five subpopulations displayed a high level of glycolysis. After expansion, genes related to glycolysis were globally upregulated across the subpopulations. HFIV showed the highest enrichment in metabolism process. All HF compartments except for HFSC scored lower for quiescence, indicating that expansion induced the activated state in these groups.

Replenishment and regeneration of the skin epidermis is driven by different stem cell populations located in distinct HF compartments. To investigate which population is involved in expansion, we explored the key markers in the Hippo pathway (Figure 3C). First, compared with YAP1, the expression level and variation of Wwtr1 (TAZ) was weak, indicating that YAP1 is the main contributor in the expansion state. Second, the related genes downstream of YAP1 were overexpressed, suggesting that YAP1 activates the downstream cascade in an early stage at PD0. Furthermore, the gene expression level and the percent of cells that express that gene before and after expansion differed significantly in each subpopulation, indicating possible involvement of every population during the process. As pathway scoring showed significance in all subclusters except for HFSC, we speculated that those populations are responding rapidly and acting reactively. Previous studies of the wound healing process have reported that stem cells originating from two distinct niches and locations, namely Lgr6+ stem cells and Lgr5+ stem cells, respond differently (Joost et al., 2018). In our dataset, Lgr5+ and Lgr6+ cells were present mainly in HFSC, whereas Lgr6+ descendants were present in infundibulum, HFIII, HFIV, and HFSC (Figure 3C). *In vivo* staining verified the commitment of Lgr6+ cells in new skin generation during expansion. Additionally, the process was primed by YAP1. Taking advantage of our lineage-trace model, we next sought to investigate how the gene expression dynamics of Lgr6+ cells affect expansion.

Figure 3 Heterogeneity in the skin stem cell niche in response to expansion

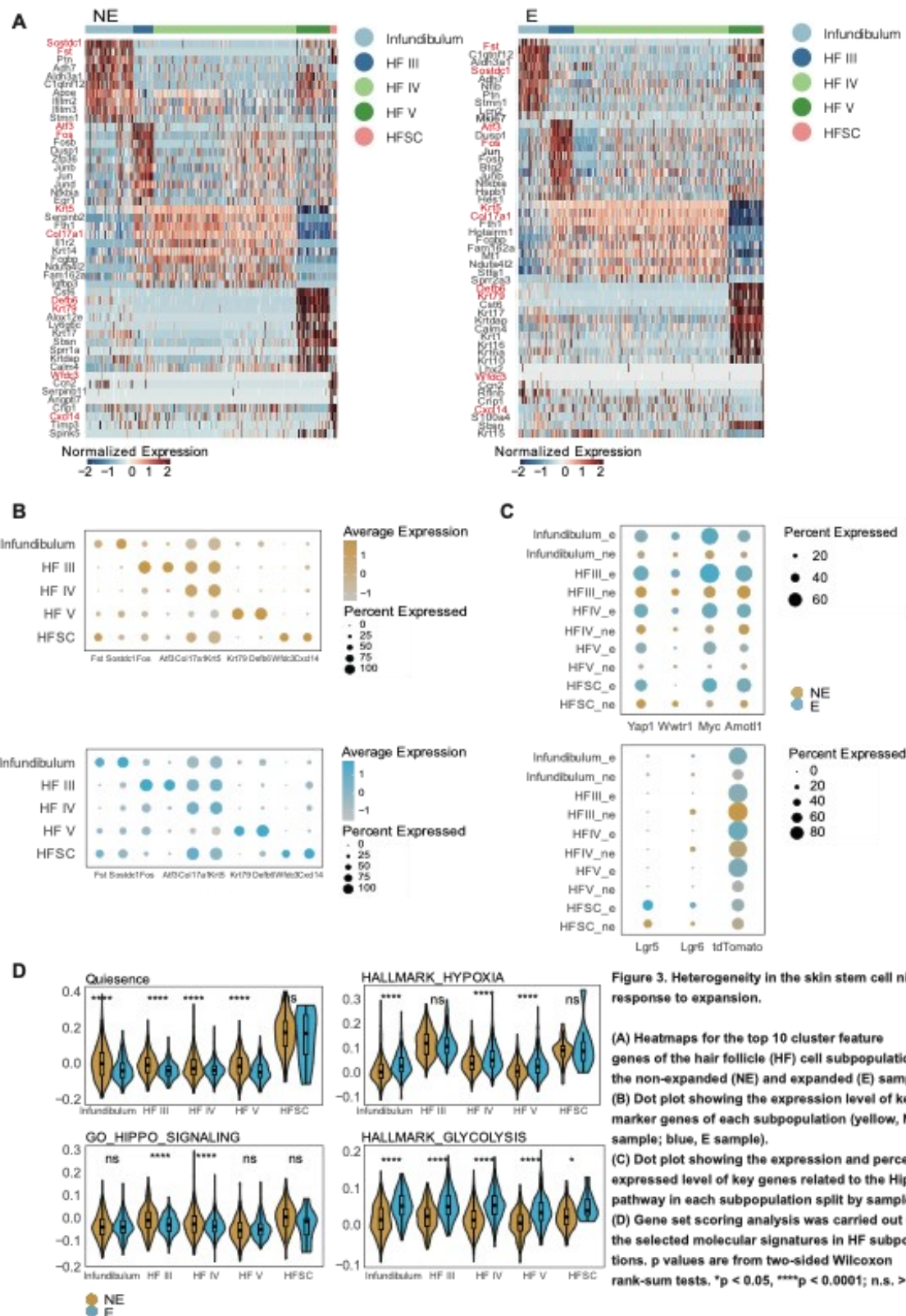


Figure 3. Heterogeneity in the skin stem cell niche in response to expansion.

(A) Heatmaps for the top 10 cluster feature genes of the hair follicle (HF) cell subpopulations in the non-expanded (NE) and expanded (E) samples. (B) Dot plot showing the expression level of key marker genes of each subpopulation (yellow, NE sample; blue, E sample). (C) Dot plot showing the expression and percent expressed level of key genes related to the Hippo pathway in each subpopulation split by sample. (D) Gene set scoring analysis was carried out using the selected molecular signatures in HF subpopulations. p values are from two-sided Wilcoxon rank-sum tests. *p < 0.05, ****p < 0.0001; n.s. > 0.05.

Pseudotemporal trajectory analysis reveals Lgr6 stem cell plasticity during skin expansion

Evidence has shown that epidermis progresses from basal layers to spinous. Having identified that the newly generated epidermis is derived mainly from Lgr6+ progenitor cells in vivo, we next asked how expansion affects the gene dynamics of the Lgr6 progenitor cells and their progeny. We first ordered Lgr6+/TdTomato- (i.e., Lgr6 progenitor) and TdTomato+ (i.e., Lgr6 progeny) cells from basal, HFIII, HFIV, and spinous I-III onto a principal component analysis plot (Figure 4A). When we assessed the imbalance score on the whole dataset, we found a globally balanced structure of cell distribution along the development axis between E and NE conditions. This result indicates that it is feasible to perform trajectory inference on the full dataset first and then split the dataset for analysis (Street et al., 2018; Van den Berge et al., 2020). This approach allows us to construct a robust and comparable trajectory on NE and E samples. Cell density estimation distribution for the two samples showed a bimodal distribution for both NE and E. For the first peak, E cells showed a tendency to move towards later pseudotime, whereas for the second peak, E cells tended to lag behind normal progression. We subsequently applied the Kolmogorov-Smirnov test on the derived pseudotime values with cell distribution ($p < 2.2\text{e-}16$), and the results confirmed a significant difference between the two. By using a negative binomial generalized additive model as described in a previous study (reference), we tested and modeled a smooth average expression profile with pseudotime for genes whose dynamics are associated with the inferred trajectory in each condition. Assessment of differentially expressed genes along pseudotime revealed more than twice as many differentially expressed genes in the NE lineage (1,314 genes) as in the E lineage (991 genes). Most of the differentially expressed genes (~84%) in the NE condition were also in the E condition. Taken together, these data demonstrate the robustness of our study and reveal a global overview and a distinct transcriptome profile for Lgr6+ cell development during the expansion state.

Differential gene expression analysis showed that 441 genes were differentially expressed between NE and E samples with a fold change greater than 2 or less than $\frac{1}{2}$. By ordering the differential expression from E and NE samples according to hierarchical clustering and comparing the expression variation over pseudotime in NE, we found that expansion induced systematic change in transcriptional dynamics. Interestingly, the expression level for bulge marker genes Sparc, Cxcl14, and Postn are elevated during expansion (Joost et al., 2018). Genes such as Sparc and Cxcl14 reach their peak earlier than or at the same time as they do in homeostasis, and then return to NE levels in the later stage. Some genes were expressed at a level that exceeded their counterparts in the NE group along the pseudotime. This finding suggests that the Lgr6+ population has an early response to the expansion. Consistently, IFE basal cell signatures were also overexpressed during the course. Genes like Ifitm3 remained at high levels in the process, whereas other genes like Krt14, Mt2, and Ly6e were highly expressed at first and then later decreased to a level lower than that at homeostasis. Moreover, the keratinocyte differentiation marker Krtdap was found to be elevated as well. Collectively, these data suggest that during expansion, the Lgr6+ population responds quickly to evolve into the next stage, during which the cells appear to elevate their potential energy or stemness first. They begin to adapt an IFE-like identity early, but their final identity is weaker than typical IFE cells.

Figure 4 Pseudo-temporal trajectory analysis reveals Lgr6+ stem cell plasticity during skin expansion

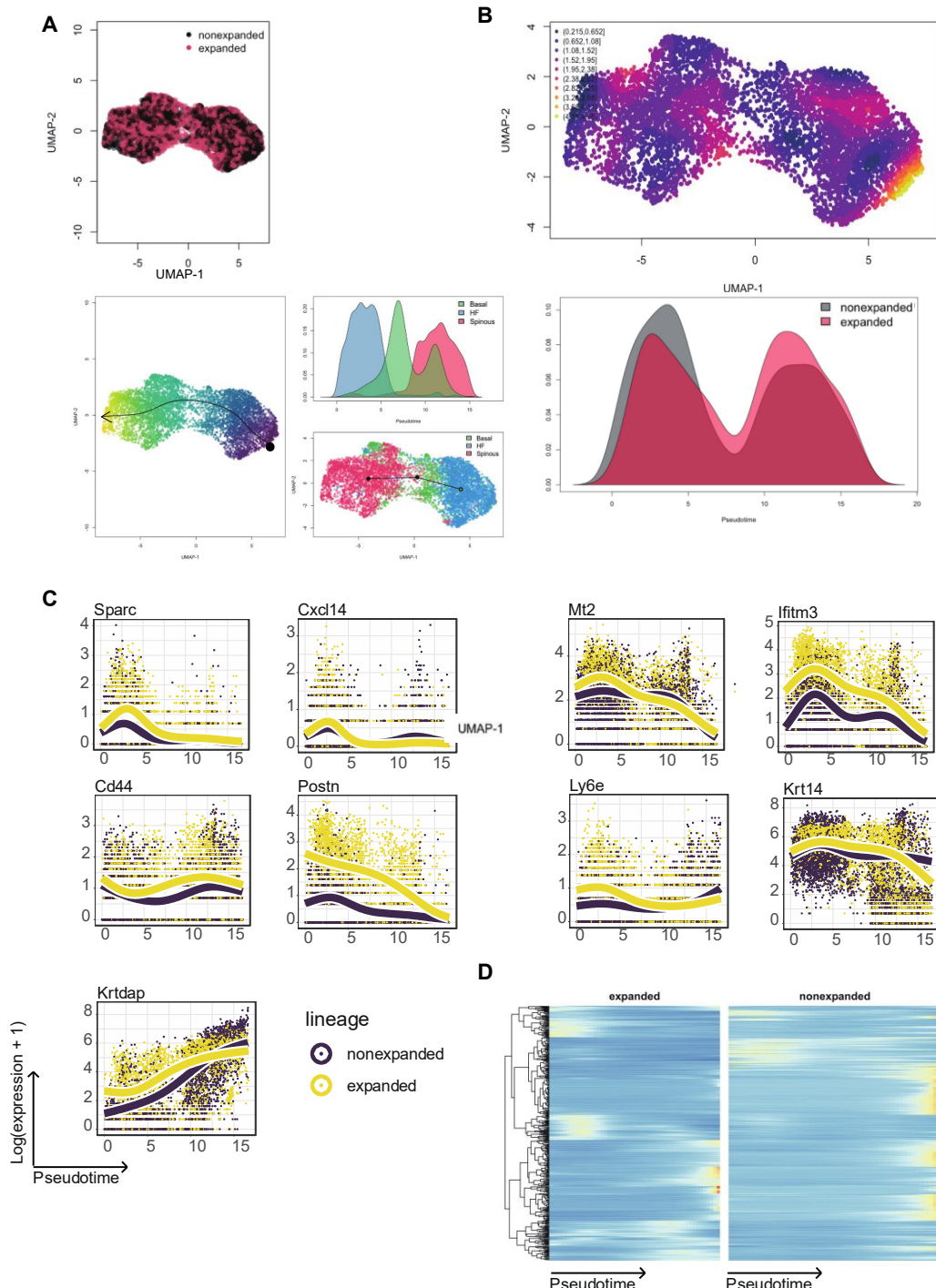


Figure 4. Pseudo-temporal trajectory analysis reveals Lgr6+ stem cell plasticity during skin expansion.
(A) Distribution of Lgr6+ progenitor and Lgr6+ progeny by uniform manifold approximation and projection (UMAP) colored by condition/cell type. Cells are distributed along the inferred trajectory.
(B) Distribution of imbalance score on a UMAP image shows the level of balance on the global development path.
(C) Density estimation of Lgr6+ progenitor and progeny along the inferred pseudo-time.
(D) Expression pattern of selected bulge/interfollicular epidermal [IFE]/differentiation markers in Lgr6+ progenitor and progeny cells with trajectory.
(E) Heatmaps of the genes differentially expressed between conditions. The differentially expressed genes are ordered according to hierarchical clustering on the expanded condition.

Conclusion

In this work, we uncover the keratinocyte transcriptome changes of an *in vivo* tissue expansion model at a single-cell level. By using a lineage-tracing model, we specifically scoped how the Lgr6+ skin stem cells adapt to stretch. We characterized a common transcriptome program within the epidermis on the cell-type level and identified the molecular signatures in the expansion state. Specifically, we found that glycolysis and the HIF-1 signaling pathway were upregulated while cell-cell junction and focal adhesion genes were downregulated. By analyzing the key genes and related pathway changes, and verifying these changes *in vivo*, we found that Lgr6+ cells constitute the key committed cell population for new skin generation. The underlying early key driver for this process is the Yap-related Hippo pathway. Trajectory analysis on Lgr6+ progenitor and progeny cells suggested that expansion triggered an enhanced response during the stem cell stage and weakened IFE identity as the cells matured, further supporting *in vivo* findings and generating a rich hypothesis. Taken together, this study provides a general survey of the single-cell transcriptome profiles and helps to elucidate the complex molecular process of mechanical force-induced skin expansion. Ultimately these findings will uncover the factors enabling mobilization of endogenous stem cells in the skin, allowing us to design novel therapies to improve human skin regeneration.

References

- Aragona, M., Sifrim, A., Malfait, M., Song, Y., Van Herck, J., Dekoninck, S., Gargouri, S., Lapouge, G., Swedlund, B., and Dubois, C. (2020). Mechanisms of stretch-mediated skin expansion at single-cell resolution. *Nature* 584, 268-273.
- Barker, N., Van Es, J.H., Kuipers, J., Kujala, P., Van Den Born, M., Cozijnsen, M., Haegebarth, A., Korving, J., Begthel, H., and Peters, P.J. (2007). Identification of stem cells in small intestine and colon by marker gene Lgr5. *Nature* 449, 1003-1007.
- Borreguero-Muñoz, N., Fletcher, G.C., Aguilar-Aragon, M., Elbediwy, A., Vincent-Mistiaen, Z.I., and Thompson, B.J. (2019). The Hippo pathway integrates PI3K–Akt signals with mechanical and polarity cues to control tissue growth. *PLoS biology* 17, e3000509.
- Butler, A., Hoffman, P., Smibert, P., Papalex, E., and Satija, R. (2018). Integrating single-cell transcriptomic data across different conditions, technologies, and species. *Nature biotechnology* 36, 411-420.
- Cheng, J.B., Sedgewick, A.J., Finnegan, A.I., Harirchian, P., Lee, J., Kwon, S., Fassett, M.S., Golovato, J., Gray, M., and Ghadially, R. (2018). Transcriptional programming of normal and inflamed human epidermis at single-cell resolution. *Cell reports* 25, 871-883.
- Cheung, T.H., and Rando, T.A. (2013). Molecular regulation of stem cell quiescence. *Nature reviews Molecular cell biology* 14, 329-340.
- Dobrokhoto, O., Samsonov, M., Sokabe, M., and Hirata, H. (2018). Mechanoregulation and pathology of YAP/TAZ via Hippo and non-Hippo mechanisms. *Clinical and translational medicine* 7, 1-14.
- Fuchs, E. (2008). Skin stem cells: rising to the surface. *The Journal of cell biology* 180, 273-284.
- Gao, D., Joshi, N., Choi, H., Ryu, S., Hahn, M., Catena, R., Sadik, H., Argani, P., Wagner, P., and Vahdat, L.T. (2012). Myeloid progenitor cells in the premetastatic lung promote metastases by inducing mesenchymal to epithelial transition. *Cancer research* 72, 1384-1394.
- Green, H. (1977). Terminal differentiation of cultured human epidermal cells. *Cell* 11, 405-416.
- Gurkar, A.U., Chu, K., Raj, L., Bouley, R., Lee, S.-H., Kim, Y.-B., Dunn, S.E., Mandinova, A., and Lee, S.W. (2013). Identification of ROCK1 kinase as a critical regulator of Beclin1-mediated autophagy during metabolic stress. *Nature communications* 4, 1-13.
- Gutschner, T. (2013). The noncoding RNA MALAT1 is a critical regulator of the metastasis phenotype of lung cancer cells. *Cancer res* 73, 1180-1189.
- Haensel, D., Jin, S., Sun, P., Cinco, R., Dragan, M., Nguyen, Q., Cang, Z., Gong, Y., Vu, R., and MacLean, A.L. (2020). Defining epidermal basal cell states during skin homeostasis and wound healing using single-cell transcriptomics. *Cell reports* 30, 3932-3947. e3936.
- Iskratsch, T., Wolfenson, H., and Sheetz, M.P. (2014). Appreciating force and shape—the rise of mechanotransduction in cell biology. *Nature reviews Molecular cell biology* 15, 825-833.
- Ito, M., Liu, Y., Yang, Z., Nguyen, J., Liang, F., Morris, R.J., and Cotsarelis, G. (2005). Stem cells in the hair follicle bulge contribute to wound repair but not to homeostasis of the epidermis. *Nature medicine* 11, 1351-1354.

- Joost, S., Annusver, K., Jacob, T., Sun, X., Dalessandri, T., Sivan, U., Sequeira, I., Sandberg, R., and Kasper, M. (2020). The molecular anatomy of mouse skin during hair growth and rest. *Cell stem cell* 26, 441-457. e447.
- Joost, S., Jacob, T., Sun, X., Annusver, K., La Manno, G., Sur, I., and Kasper, M. (2018). Single-cell transcriptomics of traced epidermal and hair follicle stem cells reveals rapid adaptations during wound healing. *Cell reports* 25, 585-597. e587.
- Joost, S., Zeisel, A., Jacob, T., Sun, X., La Manno, G., Lönnerberg, P., Linnarsson, S., and Kasper, M. (2016). Single-cell transcriptomics reveals that differentiation and spatial signatures shape epidermal and hair follicle heterogeneity. *Cell systems* 3, 221-237. e229.
- Karaman, R., and Halder, G. (2018). Cell junctions in Hippo signaling. *Cold Spring Harbor perspectives in biology* 10, a028753.
- Macosko, E.Z., Basu, A., Satija, R., Nemesh, J., Shekhar, K., Goldman, M., Tirosh, I., Bialas, A.R., Kamitaki, N., and Martersteck, E.M. (2015). Highly parallel genome-wide expression profiling of individual cells using nanoliter droplets. *Cell* 161, 1202-1214.
- Madisen, L., Zwingman, T.A., Sunkin, S.M., Oh, S.W., Zariwala, H.A., Gu, H., Ng, L.L., Palmiter, R.D., Hawrylycz, M.J., and Jones, A.R. (2010). A robust and high-throughput Cre reporting and characterization system for the whole mouse brain. *Nature neuroscience* 13, 133.
- Nava, M.M., Miroshnikova, Y.A., Biggs, L.C., Whitefield, D.B., Metge, F., Boucas, J., Vihinen, H., Jokitalo, E., Li, X., and Arcos, J.M.G. (2020). Heterochromatin-driven nuclear softening protects the genome against mechanical stress-induced damage. *Cell* 181, 800-817. e822.
- Neumann, C.G. (1957). The expansion of an area of skin by progressive distention of a subcutaneous balloon: use of the method for securing skin for subtotal reconstruction of the ear. *Plastic and reconstructive surgery* 19, 124-130.
- Pedersen, E., Wang, Z., Stanley, A., Peyrollier, K., Rösner, L.M., Werfel, T., Quondamatteo, F., and Brakebusch, C. (2012). RAC1 in keratinocytes regulates crosstalk to immune cells by Arp2/3-dependent control of STAT1. *Journal of cell science* 125, 5379-5390.
- Romani, P., Valcarcel-Jimenez, L., Frezza, C., and Dupont, S. (2020). Crosstalk between mechanotransduction and metabolism. *Nature Reviews Molecular Cell Biology*, 1-17.
- Snippert, H.J., Van Der Flier, L.G., Sato, T., Van Es, J.H., Van Den Born, M., Kroon-Veenboer, C., Barker, N., Klein, A.M., Van Rheenen, J., and Simons, B.D. (2010). Intestinal crypt homeostasis results from neutral competition between symmetrically dividing Lgr5 stem cells. *Cell* 143, 134-144.
- Street, K., Risso, D., Fletcher, R.B., Das, D., Ngai, J., Yosef, N., Purdom, E., and Dudoit, S. (2018). Slingshot: cell lineage and pseudotime inference for single-cell transcriptomics. *BMC genomics* 19, 1-16.
- Tang, Y., Rowe, R.G., Botvinick, E.L., Kurup, A., Putnam, A.J., Seiki, M., Weaver, V.M., Keller, E.T., Goldstein, S., and Dai, J. (2013). MT1-MMP-dependent control of skeletal stem cell commitment via a β 1-integrin/YAP/TAZ signaling axis. *Developmental cell* 25, 402-416.
- Tello, D., Balsa, E., Acosta-Iborra, B., Fuertes-Yebra, E., Elorza, A., Ordóñez, Á., Corral-Escariz, M., Soro, I., López-Bernardo, E., and Perales-Clemente, E. (2011). Induction of the mitochondrial NDUFA4L2 protein by HIF-1 α decreases oxygen consumption by inhibiting Complex I activity. *Cell metabolism* 14, 768-779.

- Tong, L., Corrales, R.M., Chen, Z., Villarreal, A.L., De Paiva, C.S., Beuerman, R., Li, D.-Q., and Pflugfelder, S.C. (2006). Expression and regulation of cornified envelope proteins in human corneal epithelium. *Investigative ophthalmology & visual science* *47*, 1938-1946.
- Toruner, G.A., Ulger, C., Alkan, M., Galante, A.T., Rinaggio, J., Wilk, R., Tian, B., Soteropoulos, P., Hameed, M.R., and Schwalb, M.N. (2004). Association between gene expression profile and tumor invasion in oral squamous cell carcinoma. *Cancer genetics and cytogenetics* *154*, 27-35.
- Van den Berge, K., De Bezieux, H.R., Street, K., Saelens, W., Cannoodt, R., Saeys, Y., Dudoit, S., and Clement, L. (2020). Trajectory-based differential expression analysis for single-cell sequencing data. *Nature communications* *11*, 1-13.